



Synthesis of methanol using copper-*f* block element bimetallic oxides as catalysts and greenhouse gases (CO₂, CH₄) as feedstock



J.B. Branco ^{*}, A.C. Ferreira, A.P. Gonçalves, C.O. Soares, T. Almeida Gasche

Centro de Ciências e Tecnologias Nucleares (C²TN), Centro Tecnológico e Nuclear (CTN) – Instituto Superior Técnico (IST) – Universidade de Lisboa, Estrada Nacional 10, ao km 139,7, 2695-066 Bobadela LRS, Portugal

ARTICLE INFO

Article history:

Received 22 April 2016

Revised 9 June 2016

Accepted 10 June 2016

Available online 4 July 2016

Keywords:

Methanol

CO₂ and CH₄

Copper

f block elements

Intermetallic compounds

ABSTRACT

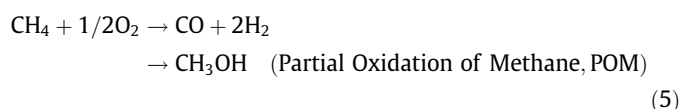
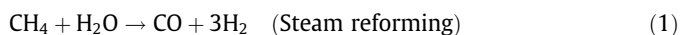
The study of methanol production using copper-*f* block element bimetallic oxides as catalysts was undertaken. Carbon dioxide and hydrogen were used as reagents, but the addition of methane to this mixture was also studied. Catalysts were obtained by two methods: (i) Controlled oxidation of binary copper-*f* block element intermetallic compounds (IC) to obtain IC bimetallic oxides and (ii) impregnation followed by controlled oxidation to obtain copper-*f* block element oxide catalysts supported on alumina. Both types of catalysts proved to be more active for the production of methanol than a commercial Cu based catalysts (Alfa Aesar, 45776-0500). The selectivity is also very high (>90%), but the incorporation of CH₄ to the feedstock has a negative effect on the catalyst behavior. The best result was that obtained with copper-cerium IC bimetallic oxide, its intrinsic activity ($\approx 900 \text{ mL}_{\text{CH}_3\text{OH}}/\text{m}^2_{\text{Cu}}\cdot\text{h}$) is 2–9 times higher in comparison with the numbers reported in the literature. To our knowledge, copper-*f* block element bimetallic oxides were never tested for the synthesis of methanol and the results herein reported are new and among the best reported until now.

© 2016 Elsevier Inc. All rights reserved.

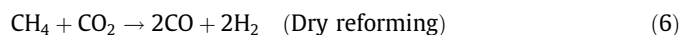
1. Introduction

The synthesis of methanol from CO₂ is particularly interesting, not only as a way to mitigate this greenhouse gas, but also due to the potential of CO₂ as an alternative and economical feedstock for the production of value-added chemicals [1–3]. Therefore, the activation of CO₂ and its hydrogenation to alcohols or other hydrocarbon compounds address simultaneously two internationally important issues: recycle of CO₂ and depletion of fossil fuels [4].

On the other hand, methane is an available and abundant feedstock, main component of natural gas that can be converted to syn-gas (hydrogen and carbon monoxide) and commercially used to produce methanol in two steps [5]: (i) Step 1, natural gas is converted into mixture of carbon monoxide, carbon dioxide and hydrogen (Eqs. (1) and (2)); and (ii) Step 2, synthesis gas is catalytically converted into methanol (Eqs. (3) and (4)). Conventional steam reforming is the simplest and commonly used route to synthesis gas production, but this process results in an excess of hydrogen. Methanol could be also produced through the partial oxidation of methane (Eq. (5)).



Alternatively, dry reforming of methane could be also a valuable option in the case of natural gas sources containing substantial amounts of CO₂ and any excess of hydrogen produced during conventional steam reforming could react with carbon dioxide or be added to the dry reforming to, ideally, produce more methanol (Eqs. (6) and (7)).



The potential use of methanol as fuel is also well known [6]. Many research groups are working on a single stage process for the manufacture of methanol. The partial oxidation route (Eq. (5)) offers a single step reaction and the advantage of directly converting methane to methanol [7,8,2]. Studies for a single step reaction via

^{*} Corresponding author.

dry reforming are scarce and to our knowledge limited to the production of C2 hydrocarbons (ethylene, ethane) [9].

In the last decades, several reviews addressing the synthesis of methanol have been reported in the literature [10–14]. Liu et al. [10] reviewed the advances in catalysts for methanol synthesis via hydrogenation of CO and CO₂; Wang et al. [11] briefly discussed methanol production from CO₂; Waugh [12], Ganesh [13] and Vaidya et al. [14] present a comprehensive overview of important investigations on CO₂ conversion to methanol. Methanol is typically produced over copper based catalysts (Cu/ZnO/Al₂O₃) at high pressures (50–100 bar) and temperatures of a few hundred degrees C (200–300 °C). However, the preparation of catalytically active “copper catalyst” as well as the nature of their active site is, even today, not entirely understood [15]. Industrial Cu/ZnO-based catalysts are prepared by a co-precipitation method [16], which creates porous aggregates of Cu and ZnO nanoparticles (NPs), with size around 10 nm and large Cu surface area, up to ~40 m² g⁻¹ when enriched copper molar compositions (Cu:Zn ~ 70:30) are used [17]. Industrial catalysts contain low amounts of a refractory oxide as structural promoter [18], in most cases up to ~10% Al₂O₃ in their composition, and their activity depends both on the specific area and Cu accessibility. Activity, normally increases with both parameters [19,20]. Methanol synthesis over Cu appears to be also a structure-sensitive reaction [16,21,22]. Another important factor is the presence of ZnO, which is responsible for the increase in the activity of Cu-based methanol synthesis catalysts [23,16]. ZnO has the function of a physical spacer between Cu nanoparticles, which helps its dispersion during the catalyst preparation and favors the synthesis of Cu catalysts with high surface areas [17].

It is also known that the role of CO is that of a reducing agent (formation of metallic Cu). Furthermore, it was also observed that the addition of CO₂ to the syngas gaseous feed increases methanol yield. CO₂ can be added up to 30% to the syngas mixture [24] and today much efforts address the conversion of pure CO₂ to methanol. However, as reported by Klier et al. [25] the production of methanol is promoted even with low concentrations of CO₂ in CO/H₂ gaseous feed, but high concentrations of CO₂ have an inhibited effect. Chinchin et al. [26] using isotope-labeled ¹⁴CO₂ confirmed that most of the methanol was produced from CO₂, whereas Sahibzada found that it is not the excess of CO₂ that is responsible for inhibition of methanol synthesis [27]. Instead it is the progressive and increased formation of water (Eq. (4)) that inhibits the formation of methanol at high concentrations of CO₂. Recently, the active sites for the activation of CO₂ and synthesis of methanol over Cu/ZnO/Al₂O₃ were identified [15]. They consist of Cu steps decorated with Zn atoms, where the synergism between copper and zinc oxide phases is responsible for a dramatic increase in the interaction with CO₂ (the interaction of Cu alone with CO₂ is very poor) that accelerates its transformation into methanol.

Efforts have been also made to modify and improve the industrial Cu/ZnO/Al₂O₃ catalyst. As an example, CuO/ZnO/Al₂O₃ catalyst activity can be improved by the addition of Pd and the effect was attributed to the existence of a hydrogen spill over mechanism [14,28]. Clearly, methanol synthesis via hydrogenation of CO₂ remains a top issue and more recently many efforts have been also put on the development of catalysts capable of operating at low temperature and near atmospheric pressure [29,30]. However, this approach is clearly not in the scope of this work.

It was also found that catalyst composition and catalyst preparation methods have huge influence on their catalytic behavior [31]. So many other catalysts were tested for the production of methanol [32–34]. Wang et al. [32] studied the behavior of CuO/CeO₂/ and CuO/YDC/ supported on alumina (YDC means yttria-doped ceria) and found that they are more active than the classical

CuO/ZnO catalyst, which was attributed to a synergistic effect between CuO and surface oxygen vacancies of CeO₂. Mao et al. [33] studied a series of Cu/ZrO₂ catalysts and found that the presence of La favors the production of methanol and that selectivity to methanol correlates with the distribution of basic sites on the catalysts surface. Sun et al. [34] studied the conversion of CO₂ to methanol over a series of La-M-Cu-Zn-O (M = Y, Ce, Mg, Zr) based perovskite-type catalysts and found that all catalysts are highly selective to methanol.

Therefore, the presence of *f* block elements on copper-based catalysts seems to improve the production of methanol. Actinides and lanthanides oxides were already studied with success in the partial oxidation of methane and other catalytic reactions evolving hydrocarbons [35–42] and the important role of *f* block element oxides as catalytic promoters and stabilizers is well established [43]. Therefore, actinides and lanthanides bimetallic oxides are promising candidates as catalysts for the conversion of methane and carbon dioxide into value-added chemicals, but their use for the production of methanol is, to our knowledge, scarce [32–34,41].

In our laboratories we have used binary intermetallic compounds of the type LnCu₂ (Ln = La, Ce, Pr, Nd) [44], LnNi (Ln = Pr, Gd, Lu) [45], ThCu₂ and AnNi₂ (An = Th, U) [46] as copper or nickel-lanthanide or actinide bimetallic oxide catalytic precursors (e.g., 3CuO·Ln₂CuO₄ or 2MO·AnO₂, M = Cu, Ni). The bimetallic nickel-*f* block element oxides were tested in the partial oxidation of methane (POM) [47,48] and both systems demonstrated to be very active and selective for the production of synthesis gas (CH₄ conversions ≈80% and selectivity to H₂ and CO ≈80% at 750 °C). More recently, the production of light hydrocarbons (ethane and ethylene) was successfully achieved using methane as feedstock and nitrous oxide as oxidizing agent over bimetallic copper or calcium or nickel actinide oxides (Th, U) [49,50] and potassium-lanthanide chloride molten salts (KCl–LnCl₃, Ln = La, Ce, Sm, Dy and Yb) [51]. In common, all these systems have the existence of a synergism between the transition metal (Ca, Cu, Ni) and the *f* block element, that influences their catalytic behavior.

Herein, we present the behavior of two types of copper based catalysts for the production of methanol using CO₂ and H₂ as main reagents. The addition effect of CH₄ to this mixture was also studied. The first type of catalysts was obtained by controlled oxidation of copper binary intermetallic compounds (CeCu₂ and ThCu₂) and the products are IC bimetallic oxides of the type 2CuO·MO₂ (M = Ce, Th), whereas the second type of catalysts was obtained by co-precipitation replacing ZnO in the industrial Cu/ZnO-based catalysts by an *f* block element oxide (2CuO·MO_x·Al₂O₃; M = Ce, Th). All products were characterized by powder X-ray (XRD), nitrogen absorption (specific surface area, BET), H₂ temperature-programmed reduction (H₂-TPR), CO₂ temperature programmed desorption (CO₂-TPD), N₂O reactive chemisorption and scanning electron microscopy (SEM), complemented with energy dispersive X-ray spectrometry (EDS).

2. Experimental

Intermetallic compounds (IC) containing Cu and *f* block elements (LnCu₂, Ln = La, Ce and ThCu₂) were prepared by direct melting of stoichiometric amounts of the elements (Goodfellow foil, Cu 99.99+%; La, Ce 99.9%; Th 99.5%) in a homemade arc furnace equipped with a water-cooled copper crucible under dynamic high vacuum (10⁻⁵ torr). The melting process was repeated at least three times in order to ensure a perfect homogeneity. The weight losses were less than 0.5 wt.%. No further thermal treatment was needed, e.g. annealing, since all compounds melt congruently. The 2–5 g ingots were kept under nitrogen inside a glove box (H₂O and O₂ contents < 5 ppm).

To obtain the IC bimetallic oxides, IC controlled oxidation under air (mixture of 20% of O₂ in nitrogen, flow 50 mL/min) at 10 °C/min heating rate up to 900 °C was carried out in a U-shaped quartz reactor, plug flow type reactor, with a fixed bed (quartz wool) and an inside volume of 15 cm³. A mass flow controller (Bronkhorst, EL-flow series) was used to control the oxidation gas flow of 50 mL/min. For oxidation purpose, typically a 0.1 g ingot and particle size < 200 Mesh were used.

Bimetallic oxides supported on alumina – (2CuO·MO_x·Al₂O₃; M = Ce, Th) – were prepared by co-precipitation method, as described elsewhere [2]. As an example, in order to achieve the synthesis of the commercial catalyst 2CuO/CeO₂/Al₂O₃, aqueous solutions of the Cu(NO₃)₂·2.5H₂O (0.4 M), Ce(NO₃)₃·6H₂O (0.2 M) and Al(NO₃)₃·9H₂O (0.2 M) were prepared and mixed under constant and vigorous stirring and heating. When the solution reached 80 °C, a KOH solution (0.50 M) was slowly added until the correspondent hydroxides precipitates – pH of the solution was kept in the 9.5–10.5 range. The precipitate was then aged for 48 h, filtered and washed with distilled water until the pH of the solution reached 7.5. The sample was dried at 100 °C overnight, crushed and calcined in air at 400 °C for 4 h to yield the desired catalysts. The same procedure was followed to prepare all the other supported catalysts in alumina. Deionized water and metallic precursors were used as received (purity > 99.99%).

Specific surface areas (BET method; single point relative pressure $P/P_0 = 0.3$ using a mixture of 30% nitrogen in helium, flow 20 mL/min) were obtained on a Micromeritics ChemSorb 2720 instrument equipped with a high temperature module option (APX). Prior to measurements, all samples were degassed at 250 °C for 2 h under N₂. CO₂-TPD, N₂O chemisorption and H₂-TPR, including quantification, were also recorded on this instrument.

Copper surface area was estimated from the reactive chemisorption of N₂O at 80 °C using the combined method described by Gervasini [52,53]. This method is based on the measurement of H₂ consumption during temperature programmed-reduction (H₂-TPR) after surface oxidation by N₂O. Preceding the analysis, catalyst copper oxide phase is selectively reduced to Cu under a 10%H₂/argon mixture (heating up to 500 °C, at 10 °C/min, flow 50 mL/min, $m \approx 70$ –90 mg). Subsequently, a two-step analysis consisting of (i) N₂O oxidation of Cu to Cu₂O and (ii) H₂ temperature-programmed-reduction in the formed Cu₂O surface species (H₂-TPR) is performed. This analysis was done on the Micromeritics ChemSorb 2720 instrument and the conditions for step 1 (at 80 °C during 30 min with a mixture of 10% N₂O/helium, total flow 50 mL/min) were previously optimized (supplementary material, Figs. S1 and S2) for such apparatus. After temperature decrease to 20 °C and cleaning with a pure He stream (50 mL/min) for 30 min, the second step is then performed by heating up to 500 °C at a rate of 10 °C/min under the 10%H₂/argon mixture. Experiments were repeated as a function of N₂O partial pressure in the gaseous phase and temperature of activation (Step 1) and we have found that H₂ consumption (Step 2) is constant and independent of the N₂O partial pressure (Fig. S1), whereas the appropriate temperature for surface oxidation with N₂O is between 60 and 140 °C since bulk oxidation of metallic copper was only detected for temperatures >160 °C. Fig. S2 shows clearly a peak at ≈ 300 °C very near to the reduction temperature of bulk CuO (≈ 340 °C, not shown). Quantitative H₂-uptakes were evaluated by integration of the experimental H₂-TPR curves, based on previous calibration measurements with the CuO powder (Aldrich, 99.99995% purity) used in this studies (see supplementary material, Fig. S3).

CO₂-TPD was recorded using a two-step methodology: (i) before analysis, all catalysts (20–100 mg) were saturated with CO₂ (20 mL/min) at 50 °C for 1 h, followed by cleaning with a pure

He stream (50 mL/min) at the saturation temperature for 2 h; and (ii) once a stable line was obtained, chemisorbed CO₂ was desorbed by heating from 50 °C up to 1000 °C at a rate of 10 °C/min under a pure He stream (20 mL/min).

XRD patterns were obtained in reflection geometry with a PANalytical X'Pert Pro diffractometer using Cu, $\kappa\alpha$ monochromatic radiation ($\lambda = 1.5406$ Å). The operational settings for all scans were as follows: voltage = 40 kV; current = 35 mA; 2θ scan range 19–81° using a step size of 0.03° at a scan speed of 0.003°/s. For identification purposes, the relative intensities (I/I_0) and the d -spacing (Å) were compared with standard JCPDS powder diffraction files [54]. The particle size was determined by means of the Scherrer's equation [55]. Surface morphology was recorded using a FE-SEM JEOL JSM-6500F, operating at 15–20 keV and 80 A. The chemical composition was determined by EDS, using a B-U Bruker Quantax 400 EDS system (supplementary material, Table S1).

Catalytic tests were carried out in a U-shaped stainless steel plug-flow reactor (316S, 350 mm length, 10 mm diameter), with a fixed bed (Pyrex wool) and an internal volume of 15 cm³. Catalyst grain size was controlled using a 200 Mesh sieve (0.074 mm), $m = 30$ –110 mg. Mass flow controllers (Bronkhorst, EL-flow series) were used to control CH₄, CO₂, H₂ and He flows, whereas the reactor outlet pressure was controlled using a Bronkhorst EL-series digital electronic pressure controller. Gaseous mixtures of CO₂/H₂ (1:3 mol/mol) or CO₂/H₂/CH₄ (1:3:1 mol/mol/mol) were used and the reaction was studied with an adequate Gas Hourly Space Velocity (GHSV, mL of CO₂ converted per g of catalyst and per h) of 5000–80000 (typically 40000). Unless otherwise stated, 50 bars and 250 °C were used as standard conditions. The reactor outlet gas composition was online analyzed by gas chromatography using two Agilent systems: first, 7820A GC equipped with a flame ionizing detector (FID) and a HP-PLOT-U capillary column ($L = 30$ m, 1/8 in., ID = 0.32 mm) for the detection of methanol and other condensable products and, second, 4890D GC equipped with a thermal conductivity detector (TCD) and a Restek ShinCarbon ST column ($L = 2.0$ m, 1/8 in., ID = 1 mm, 100/200 mesh) for the detection of all gaseous reagents and products. Each system uses a 6-port gas sampling valve with a 0.250 mL loop. Additionally, before TCD analysis the outlet gas was cooled in an ice-water trap in order to avoid column contamination, namely by water. Unless stated otherwise, all pure gases and mixtures were purchased from Air Liquide and supplied with a Alphagaz 2 purity.

The intrinsic activity (IA) was defined as the volume of methanol formed per m² of copper per hour (mL_{CH₃OH}/m_{Cu}²·h). Unless otherwise stated, the values reported in this paper represent the steady state activities after 1 h on stream. For mixture A (CO₂ + 3H₂), the conversion of CO₂, selectivity to CH₃OH, CO and C₂ (C₂H₄ + C₂H₆) were calculated as follows: Conv. CO₂ (%) = $\frac{([CO_2]_i - [CO_2]_o)}{[CO_2]_i} \times 100$; Sel.CH₃OH (%) = $\frac{[CH_3OH]_o}{([CO_2]_i - [CO_2]_o)} \times 100$; Sel.CO (%) = $\frac{[CO]_o}{([CO_2]_i - [CO_2]_o)} \times 100$ and Sel.C₂ (%) = $\frac{2 \times [C_2]_o}{([CO_2]_i - [CO_2]_o)} \times 100$, where [CO₂]_i is the inlet flow rate of carbon dioxide and [CO₂]_o, [CO]_o and [C₂]_o are outlet flow rates of carbon dioxide, carbon monoxide and C₂ hydrocarbons. For mixture B (CO₂ + CH₄ + 3H₂), the conversion of CH₄, selectivity to CH₃OH, CO and C₂ (C₂H₄ + C₂H₆) were calculated as follows: Conv.CH₄ (%) = $\frac{([CH_4]_i - [CH_4]_o)}{[CH_4]_i} \times 100$; Sel.CH₃OH (%) = $\frac{[CH_3OH]_o}{([CH_4]_i - [CH_4]_o)} \times 100$; Sel.CO (%) = $\frac{[CO]_o}{([CO_2]_i - [CO_2]_o)} \times 100$ and Sel.C₂ (%) = $\frac{2 \times [C_2]_o}{([CH_4]_i - [CH_4]_o)} \times 100$, where [CH₄]_i is the inlet flow rate of methane and [CH₄]_o, [CO]_o and [C₂]_o are outlet flow rates of methane, carbon monoxide and C₂ hydrocarbons. Detector calibration was guaranteed using external reference mixtures of all reagents (CH₄, CO₂, H₂) and expected products (CH₃OH, C₂H₅OH, CO, C₂ hydrocarbons). The confidence level was better than 95%. For comparison purposes, a commercial copper based methanol synthesis catalyst (Alfa Aesar,

Product ID: 45776; Certificate of Analysis, wt.%: CuO 63.5, ZnO 24.7, Al₂O₃ 10.1 and MgO 1.3) was purchased and used as received.

3. Results and discussion

3.1. Catalyst characterization

IC bimetallic oxides and bimetallic oxides supported on alumina were characterized by powder X-ray diffraction (Figs. 1 and 2, respectively). The oxide phases observed are those expected (only representative cases are shown), which were confirmed by the standard JCPDS powder diffraction files [54]; namely: CuO, La₂CuO₄, CeO₂ and ThO₂ for the IC bimetallic oxides; CuO, ZnO, CeO₂ and ThO₂ for the bimetallic oxides supported on alumina. After reaction, the main change is the reduction of Cu²⁺ to Cu⁰, but in the case of the lanthanum catalyst such reduction is observed for the CuO phase and for the La₂CuO₄ ternary oxide phase with formation of Cu⁰ and La₂O₃. Other oxide phases subject to reduction, e.g. ZnO, CeO₂, show good stability under the experimental conditions employed.

These results agree with those reported by other authors that studied the synthesis of methanol over copper-*f* block compounds [56]. So it can be said that all binary copper-*f* block element intermetallic compounds act mainly as catalyst precursors since during reaction and due to the presence of H₂ they undergo reduction in the copper oxide phase (formation of Cu). Moreover, in the case of the commercial catalyst, the reduction of Cu²⁺ to Cu⁰ was also observed but not the reduction of ZnO (the XRD patterns observed after reaction are only those of Cu and ZnO, data not shown).

SEM images show that IC bimetallic oxide catalysts have a smooth surface morphology, which is built upon the aggregation of small particles (Fig. 3), whereas the bimetallic oxides supported on alumina have a rough surface and particles that present a random morphology (Fig. 4). EDS mapping confirms that, in both types of samples, metals are homogeneously distributed at the catalyst surface.

Figs. 5 and 6 show selected H₂-TPR profiles for the fresh IC bimetallic oxides and co-precipitation bimetallic oxides supported on alumina, respectively. The reduction profile of pure CuO is characterized by a single peak at 373 °C (Fig. 5), in agreement with other results reported before [57]. ThO₂ and CeO₂ reduction does not occur in this temperature range [46], which is confirmed by XRD data obtained after H₂-TPR. IC bimetallic oxides present a one-step reduction profile assigned to the reduction of the copper oxide phase that takes place at higher reduction temperatures than that observed for the Cu commercial catalyst.

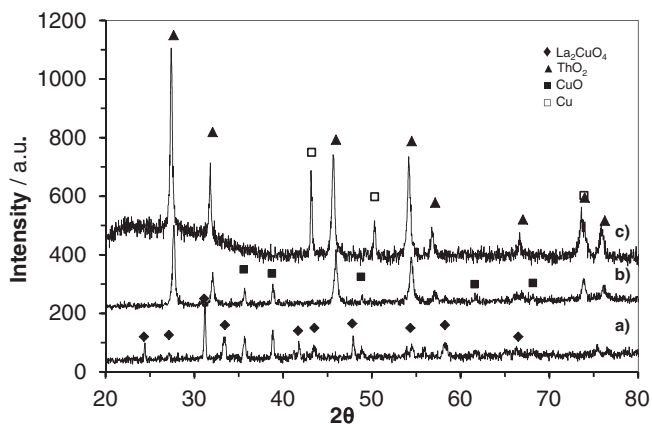


Fig. 1. IC bimetallic oxides X-ray diffraction patterns: (a and b) before reaction, 3CuO-La₂CuO₄ and 2CuO-ThO₂, respectively; (c) after reaction, 2CuO-ThO₂.

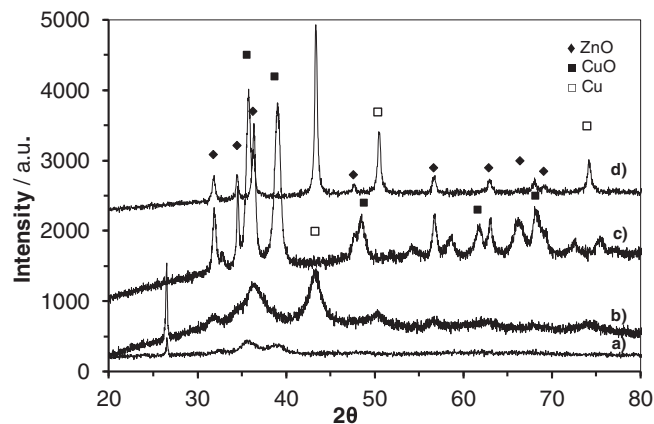


Fig. 2. Bimetallic oxides supported on alumina X-ray diffraction patterns: (a and c) before reaction and (b and d) after reaction for Cu commercial and 2CuO-ZnO-Al₂O₃, respectively.

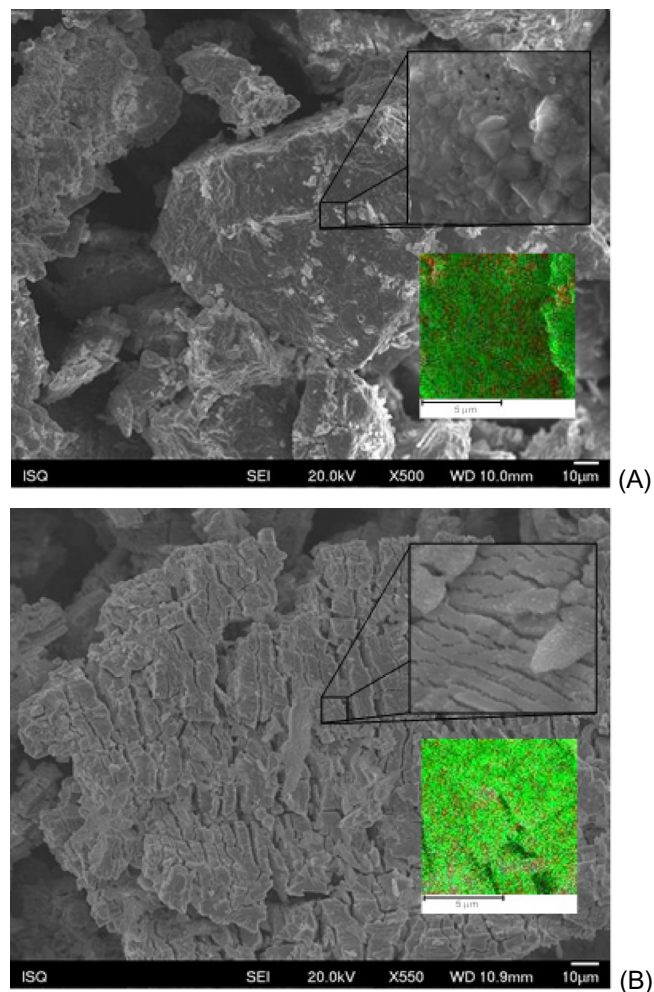


Fig. 3. SEM images of (A) 3CuO-La₂CuO₄ and (B) 2CuO-ThO₂ before reaction (inserts 5000× magnification; EDS maps: red copper; f block element green).

In contrast, the bimetallic oxides supported on alumina present a more obvious two-step reduction profile, pointing to the existence of two types of CuO species (Fig. 6). In the case of the IC bimetallic oxides this cannot be also excluded, especially in the case of CuO-ThO₂ that presents a broad shoulder not resolved in the TPR profile. In general, the reduction temperatures of

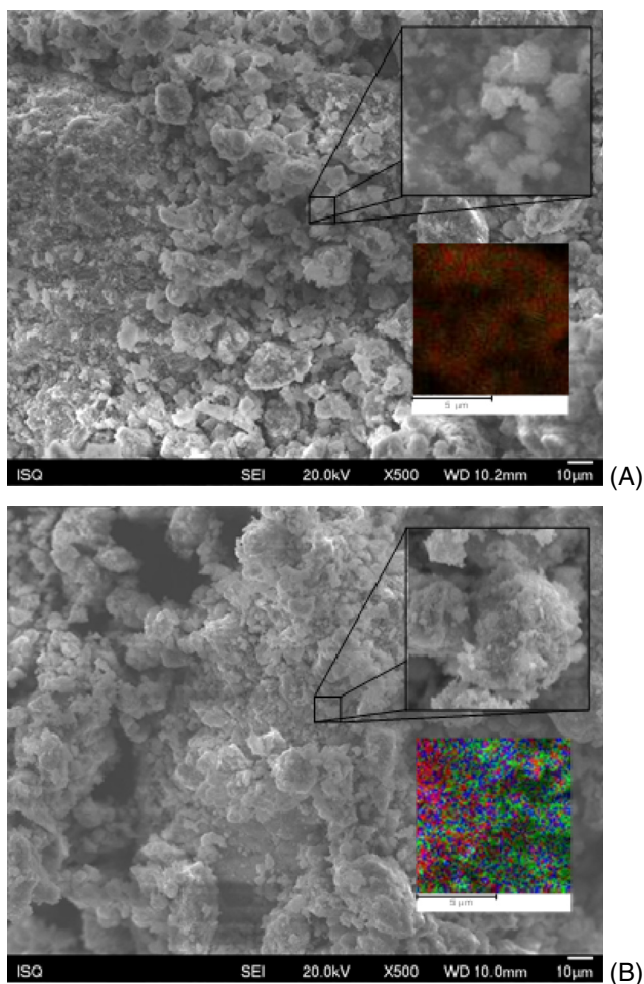


Fig. 4. SEM images of (A) $2\text{CuO}\cdot\text{ZnO}\cdot\text{Al}_2\text{O}_3$, and (B) $2\text{CuO}\cdot\text{CeO}_2\cdot\text{Al}_2\text{O}_3$ before reaction (inserts $4000\times$ magnification; EDS maps: red copper; zinc or cerium green, oxygen blue).

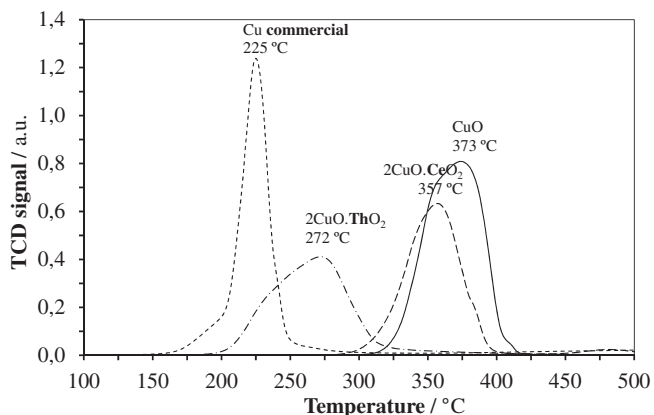


Fig. 5. H_2 -TPR profiles for the IC bimetallic oxides, Cu commercial and pure CuO.

bimetallic oxides supported on alumina are lower than those of the IC bimetallic oxides, the lowest reduction temperature being obtained for $2\text{CuO}\cdot\text{ZnO}\cdot\text{Al}_2\text{O}_3$ (191°C). All alumina supported catalysts present higher reduction temperatures than the commercial catalysts (225°C), except $2\text{CuO}\cdot\text{ZnO}\cdot\text{Al}_2\text{O}_3$. However, a comparison with pure CuO supported on alumina ($\text{CuO}\cdot\text{Al}_2\text{O}_3$) shows a

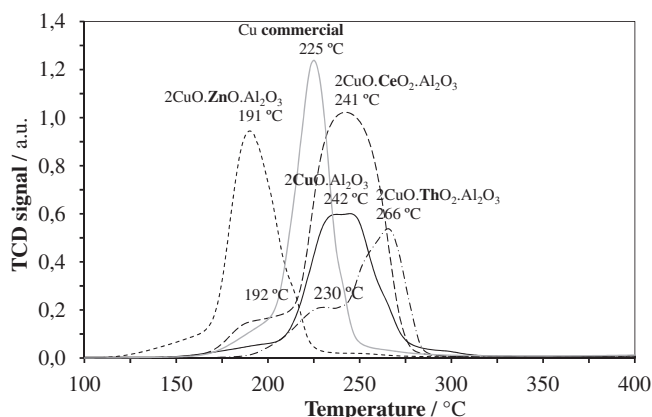


Fig. 6. H_2 -TPR for the bimetallic oxides supported on alumina, Cu commercial and CuO supported on alumina.

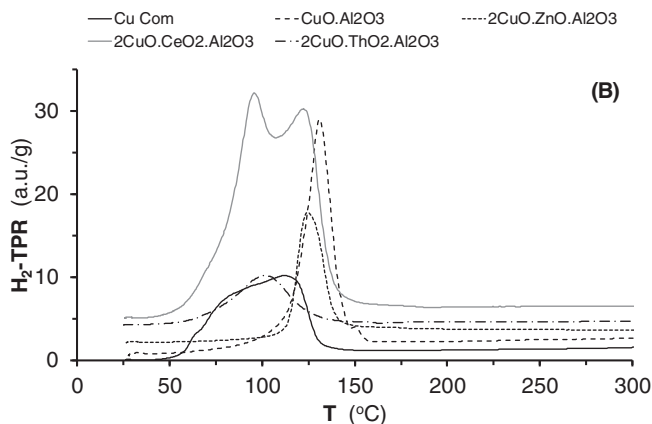
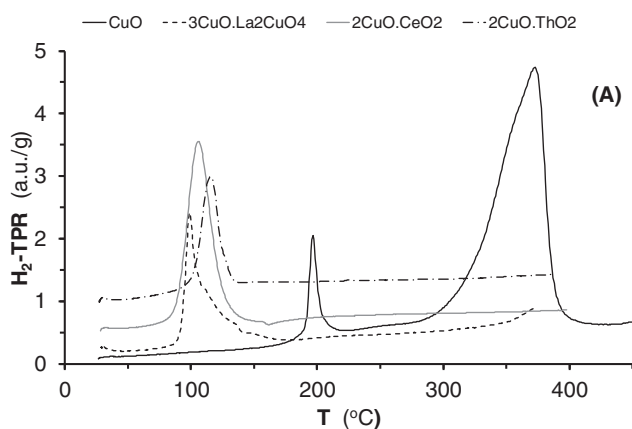


Fig. 7. H_2 -TPR after N_2O chemisorption at 80°C : (A) IC bimetallic oxides and (B) bimetallic oxides supported on alumina.

reduction behavior that in the case of the cerium based catalyst is comparable ($\approx 240^\circ\text{C}$), whereas in the case of the thorium based catalyst it is significantly higher (266 versus 242°C).

It can be concluded that all co-precipitation bimetallic oxides reduce in the same temperature range (191 – 266°C) whereas the IC bimetallic oxides reduce at higher temperatures (272 – 357°C), meaning a higher resistance toward reduction and CuO species less labile and available for oxidative catalytic processes. Moreover, the oxygen lability on the cerium based catalysts is very similar to that of pure CuO or CuO supported on alumina, whereas in the case of the thorium based catalysts it is very different and certainly will have an influence on their catalytic properties.

Table 1

Characterization of copper bimetallic oxide catalysts by XRD and SEM/EDS before reaction.

Catalyst	XRD			SEM/EDS	
	Before	After	L (nm) ^a	Cu/M ^b	Cu/Al ^c
3CuO·La ₂ CuO ₄	CuO, LaCuO ₄	Cu, La ₂ O ₃	29.1	2.8	–
2CuO·CeO ₂	CuO, CeO ₂	Cu, CeO ₂	25.2	2.3	–
2CuO·ThO ₂	CuO, ThO ₂	Cu, ThO ₂	32.1	1.9	–
Cu Commercial	CuO	Cu	33.9	2.6	3.5
2CuO·ZnO·Al ₂ O ₃	CuO, ZnO	Cu, ZnO	10.6	2.5	n.d. ^d
2CuO·CeO ₂ ·Al ₂ O ₃	CuO, CeO ₂	Cu, CeO ₂	17.8	2.1	6.2
2CuO·ThO ₂ ·Al ₂ O ₃	CuO, ThO ₂	Cu, ThO ₂	18.4	2.2	2.4
CuO·Al ₂ O ₃	CuO	Cu	18.4	–	31.8
CuO	CuO	Cu	–	–	–

^a L : CuO crystallite size (Scherrer's equation, monoclinic system hkl (111)).

^b Atomic ratios for M = La, Ce, Th, Zn. Theoretical values: Cu/M = 2.0.

^c Atomic ratios are higher than expected (Cu/Al = 1.0); a known problem due to an underestimated Al signal [61].

^d n.d., not detected.

In order to compare all catalysts and to improve the understanding of their catalytic fundamental behavior, metallic copper surface area was estimated from the reactive chemisorption of N₂O using the modified method described by Gervasini [52,53]. The obtained H₂-TPR profiles are reported in Fig. 7. They show only one peak at low temperature (100–200 °C), but in the case of pure CuO, a second peak can be observed at higher temperature which indicates that even for a selective oxidation with N₂O at 80 °C some bulk copper oxidation occurs. The low temperature peak, as suggested by Gervasini [53], was attributed to the reduction in the surface Cu₂O species formed after the reactive chemisorption of N₂O (Cu₂O + H₂ → 2Cu + H₂O) and used to determine the values of copper surface area of all the samples (the formulas are described in Refs. [54,55]).

In the case of the IC copper bimetallic oxides, the peak shape is very similar for all samples which are not the case for the copper supported catalysts on alumina, including the commercial catalyst. Commercial and supported alumina catalysts containing *f* block elements (2CuO·CeO₂·Al₂O₃ and 2CuO·ThO₂·Al₂O₃) present broader peaks (well separated in the case of the cerium sample) that could be attributed to some interactions (synergism) between copper and the *f*-block element. Tables 1 and 2 compile the characterization data obtained by XRD, BET, H₂-TPR and N₂O reactive chemisorption. EDS confirms that Cu content at surface is very close to the theoretical values.

3.2. Catalytic results

Fig. 8 shows the catalytic behavior of IC bimetallic oxides and bimetallic oxides supported on alumina for the production of methanol using either CO₂ + H₂ (1:3) or CH₄ + CO₂ + H₂ (1:1:3)

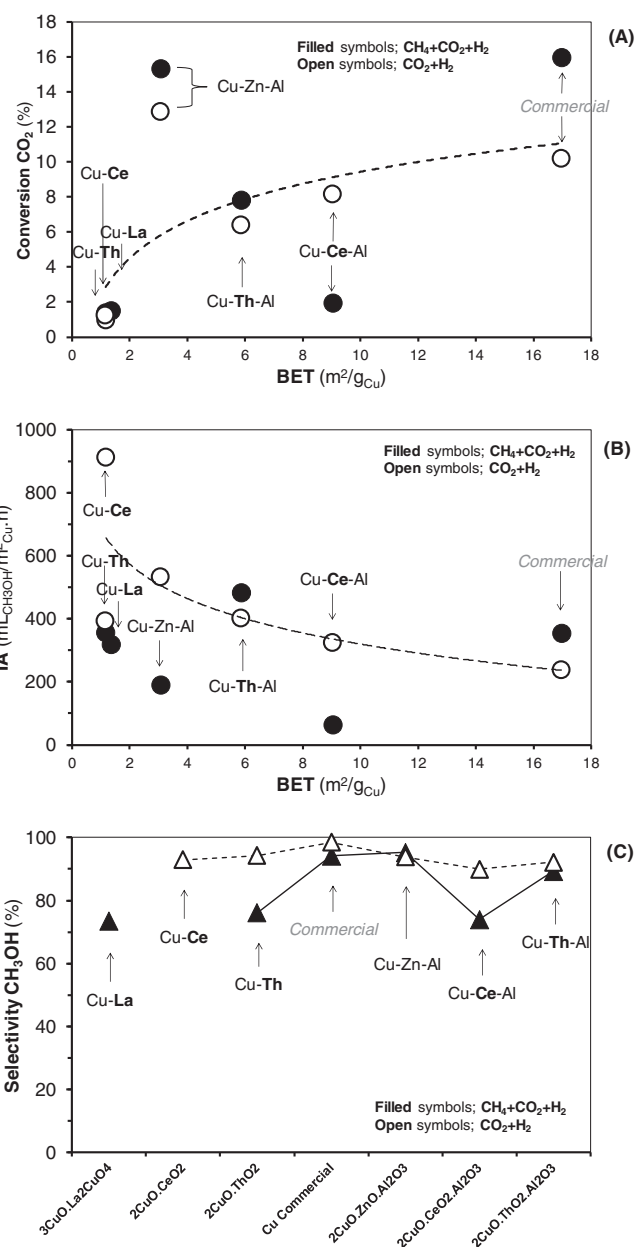


Fig. 8. Catalytic behavior of IC bimetallic oxides and bimetallic oxides supported on alumina in terms of (A) CO₂ conversion, (B) intrinsic activity (IA) and (C) methanol selectivity. Data obtained at 250 °C, 50 bar and GHSV = 40000 mL_{CO₂}/g_{cat}·h. White filled symbols, reaction CO₂ + H₂ (1:3); black filled symbols, reaction CH₄ + CO₂ + H₂ (1:1:3).

Table 2

Characterization of copper bimetallic oxide catalysts by H₂-TPR, BET and N₂O chemisorption.

Catalyst	Surface area		H ₂ -TPR (fresh)		H ₂ -TPR (after N ₂ O chemisorption)	
	m ² /g _{cat}	m ² /g _{Cu}	T _m (°C)	mol _{H₂} /mol _{cat} ^a	T _m (°C)	10 ⁻² mol _{H₂} /g _{Cu}
3CuO·La ₂ CuO ₄	2.9	1.4	–	–	99.0	7.3
2CuO·CeO ₂	5.1	1.2	357.2	481.4	106.0	6.3
2CuO·ThO ₂	2.7	1.1	272.0	–	115.0	6.1
Cu Commercial	91.3	17.0	225.0	638.8	112.0	131.7
2CuO·ZnO·Al ₂ O ₃	28.7	3.1	240.2	707.1	125.0	15.5
2CuO·CeO ₂ ·Al ₂ O ₃	78.6	9.1	208.4	242.1	122.0	35.0
2CuO·ThO ₂ ·Al ₂ O ₃	88.1	5.9	230.2	265.5	102.0	18.4
CuO·Al ₂ O ₃	25.5	4.3	244.9	–	131.0	24.7
CuO	15.3	2.1	383.0	–	194.0	0.8

^a Theoretical values between parentheses based on TPR final products (confirmed by XRD analysis): 2Cu·CeO₂; 2Cu·ThO₂; 2Cu·ZnO·Al₂O₃; 2Cu·CeO₂·Al₂O₃; 2Cu·ThO₂·Al₂O₃; Cu·Al₂O₃; Cu.

Table 3
Comparison of this work results and data from other studies using CO₂ and H₂ as reagents.

Catalyst ^a Ref.	Conversion CO ₂ (%) ^b	Yield (mL _{CH₃OH} /g _{cat} ·h) ^b	IA (mL _{CH₃OH} /m ² _{Cu} ·h) ^b	Selectivity CH ₃ OH (%) ^b
3CuO-La ₂ CuO ₄	– (1.5)	– (437.6)	– (319.4)	– (73.5)
2CuO-CeO ₂	1.0 (–)	1093.6 (–)	911.3 (–)	92.9 (–)
2CuO-ThO ₂	1.2 (1.4)	458.8 (418.3)	392.1 (357.6)	94.3 (76.1)
Cu Comm	10.2 (16.0)	4018.7 (6025.0)	236.5 (354.6)	98.4 (94.2)
2CuO-ZnO-Al ₂ O ₃	12.9 (15.3)	1641.6 (585.3)	531.3 (189.4)	93.8 (95.3)
2CuO-CeO ₂ -Al ₂ O ₃	8.1 (1.9)	2925.9 (569.6)	323.3 (62.9)	90.0 (74.0)
2CuO-ThO ₂ -Al ₂ O ₃	6.4 (7.8)	2350.5 (2826.4)	401.1 (482.3)	92.2 (89.2)
Cu/ZnO/Al ₂ O ₃ [62]	7.0 (–)	492.8 (–)	25.5 (–)	65.2 (–)
+2%Rh [62]	10.6 (–)	672.0 (–)	43.9 (–)	59.6 (–)
CZA01 [63]	19.3 (–)	– (–)	3.4 (–)	22.3 (–)
Cu-Zn-Zr-Ga-Y [59]	– (–)	2128.0 (–)	(–)	(–)
CuO-ZnO (30/70 w/w) [64]	9.8 (–)	201.6 (–)	– (–)	62.0 (–)
Cu/Zn/Ga/SiO ₂ [65]	5.6 (–)	244.2 (–)	– (–)	99.5 (–)
Cu/Ga/ZnO [66]	6.0 (–)	264.3 (–)	– (–)	88.0 (–)
Cu/ZrO ₂ [67]	6.3 (–)	250.9 (–)	– (–)	48.8 (–)
Cu/Ga/ZrO ₂ [68]	13.7 (–)	42.6 (–)	– (–)	75.5 (–)
Cu/Zn/ZrO ₂ [69]	21.0 (–)	125.4 (–)	– (–)	68.0 (–)
Ag/Zn/ZrO ₂ [69]	2.0 (–)	11.2 (–)	– (–)	97.0 (–)
Pd/Zn/ZrO ₂ [70]	6.3 (–)	24.6 (–)	– (–)	99.6 (–)

^a This work and literature best results.

^b Between parentheses the values obtained with the mixture containing methane.

mixtures as feedstock. Several conclusions can be drawn from such results:

- Conversion of CO₂ is much lower over IC bimetallic oxides when compared to that obtained over bimetallic oxides supported on alumina or the commercial catalyst (Fig. 8A);
- All copper-*f* block element oxides proved to be more active in terms of catalyst intrinsic activity for the production of methanol using CO₂ and H₂ as reagents than the commercial Cu catalyst (Fig. 8B);
- The selectivity to methanol is also very high (>90%) (Fig. 8C) and
- In general, addition of methane has a negative effect on catalytic activity and selectivity to methanol. However, it seems less pronounced over the IC bimetallic oxides (Fig. 8B and C).

A maximal IA of ≈900 mL_{CH₃OH}/m²_{Cu}·h was obtained over the copper-cerium IC bimetallic oxide, but the IA of IC bimetallic oxides and bimetallic oxides supported in alumina is higher than that measured for the commercial catalyst (reaction without methane) and 2–9 times higher than the numbers reported in the literature (Table 3). Despite the difficulty in obtaining values in the same units, comparison of our results with other relevant data shows that our catalyst has a much higher activity at comparable pressure and temperature, but at higher GHSV, than that of the Cu catalysts reported in the literature. They clearly display a remarkable catalytic behavior for the synthesis of methanol that is even more important due to the use of CO₂ and CH₄ as feedstock, which confirms the potentialities of this type of compounds.

Other factors, such as the H₂/CO₂ ratio, the reaction pressure and the gas hourly space velocity (GHSV), increase the catalyst activity, but the selectivity to methanol seems quite stable and insensitive to such parameters. Fig. 9 presents the results obtained over the copper-cerium IC bimetallic oxide.

It can be seen that increasing the hydrogen on the gaseous phase increases the catalyst activity, reaching a steady state situation at H₂/CO₂ ratios ≥ 3. Concerning the pressure, its increase leads to an increase in the catalyst activity that achieves a maximum at *P* ≥ 50 bars. Finally, catalyst IA increases in a linear way with GHSV without influence on the methanol selectivity, which confirms the nonexistence of mass or heat diffusional problems.

To our knowledge, copper-*f* block element bimetallic oxides have never been tested for the synthesis of methanol and the

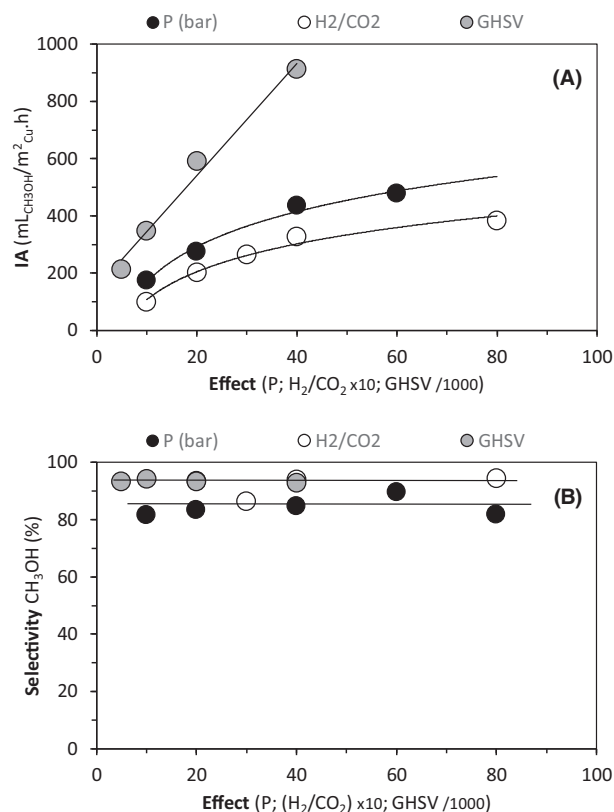


Fig. 9. Influence of the reaction parameters on the activity (A) and selectivity (B) of copper-cerium IC bimetallic oxide (2CuO-CeO₂) for the production of methanol. Data obtained at 250 °C using the mixture CH₄ + CO₂ + H₂ (1:1:3) (*P* (pressure, bar), H₂/CO₂ (molar ratio, mol/mol) and GHSV (mL_{CO₂}/m²_{Cu}·h)). Due to graphical requirements, the values of the late two parameters (H₂/CO₂ and GHSV) were multiplied by 10 and divided by 1000, respectively.

results report herein are a novelty, even when compared to those obtained over classic impregnated catalysts. Oxygen lability is an important factor that rules catalysts behavior on oxidative reactions [58]. However, in this work it seems not to be the key factor. H₂-TPR results show what seems to be an inversion correlation

between copper oxygen lability and catalyst behavior for the production of methanol: those more active tend to have oxygens that are more stable toward reduction. In the case of IC bimetallic oxides, $2\text{CuO}\cdot\text{CeO}_2$ is more active than $2\text{CuO}\cdot\text{ThO}_2$, whereas for the bimetallic oxide catalysts obtained by co-precipitation, $2\text{CuO}\cdot\text{ThO}_2\cdot\text{Al}_2\text{O}_3$ is more active than the cerium analogue, following an inverse correlation with the H_2 -TPR reduction maximum temperatures.

One possible explanation lies on the active sites and structure-activity relationships. In particular, microstrain in copper crystallites is a structural parameter that can influence the activity of Cu-based catalysts on a number of reactions, namely methanol synthesis [59]. Good catalysts were found also to have large Cu microstrain and lower crystallite size, which enhances their performance for the production of methanol. In this work, we have found that the behavior of the supported catalysts on alumina follows such trends (Fig. 10), except perhaps the Cu/Ce catalysts, whereas the neither the crystallite size nor the lattice strain seems to have a relevant influence on the methanol yield obtained over the copper-IC bimetallic oxides. In the case of data obtained for the reaction $\text{CO}_2 + 3\text{H}_2$ we can also point what it seems an inverse correlation between catalytic activity and size or lattice strain. However, further work is needed to explain this result.

Other hypotheses that may explain the performance of the copper-*f* block element bimetallic oxides include the catalysts acid-base properties or the existence of synergism between the CuO and the *f* block element oxide phase. Catalysts acid-base properties are key parameters and our results show that the basicity of the IC bimetallic oxides is very similar among them, which doesn't explain its catalytic behavior. The lower value observed for the cerium compound can be explained by the acidic contribution of the cerium oxide phase (CeO_2) that is more acid than ThO_2 [50,60]. In contrast, the basicity of the supported catalysts on alumina is higher, depends on the *f* block element and seems to be aligned with the catalyst activity for the production of methanol (Fig. 11).

IC bimetallic oxides can be described as copper oxide embedded in a matrix of lanthanide or actinide oxides with an enhanced synergism between the CuO and the *f* block element oxide phase. Higher electron density on the *d* metal has been indubitably confirmed in the case of intermetallic nickel-actinide compounds [37] and the existence of a synergism between the CuO and the *f* block element oxide phase was already recognized [49]. Therefore, in spite of less labile copper oxygen species, the IC bimetallic oxide catalytic behavior could benefit from a closer interaction between the copper and *f* block element oxide phase. Due to this proximity, an electronic share between the two metals can occur in a more efficient way, which is not the case for the catalysts obtained by

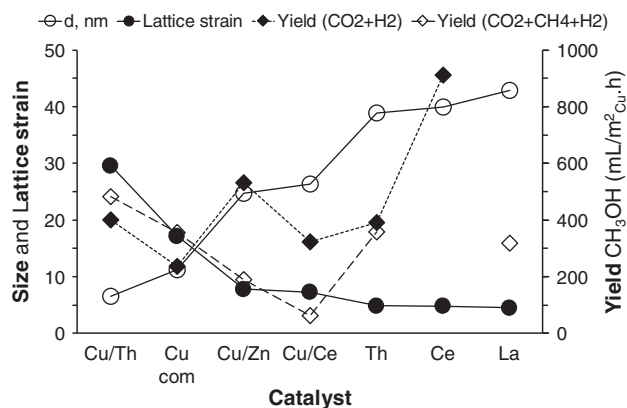


Fig. 10. Effect of the crystallite size and lattice strain on the catalysts yield to methanol. Data obtained at 250 °C, 50 bar and GHSV = 40000 mL_{CO₂}/g_{Cat}·h for both reactions: $\text{CO}_2 + \text{H}_2$ (1:3) and $\text{CH}_4 + \text{CO}_2 + \text{H}_2$ (1:1:3).

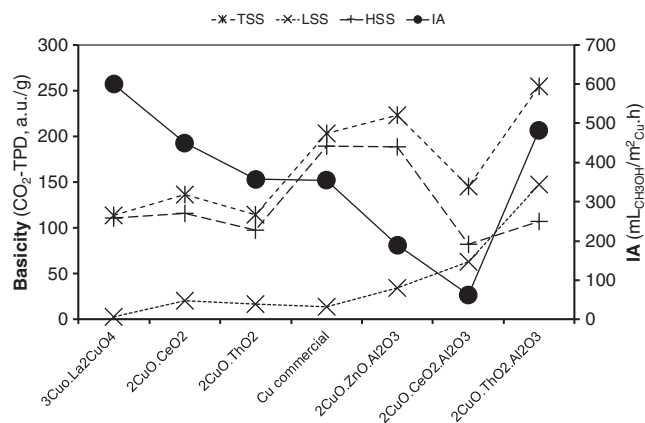


Fig. 11. Effect of the basicity on the catalysts activity and selectivity. Data obtained at 250 °C, 50 bar and GHSV = 40000 mL_{CO₂}/g_{Cat}·h using the mixture $\text{CH}_4 + \text{CO}_2 + \text{H}_2$ (1:1:3). Catalysts basic properties measured by CO_2 -TPD: TSS, LSS and HSS; total, low and high strength sites, respectively.

co-precipitation that presents much higher specific surface areas and Cu sites more disperse with smaller interaction with the *f* block element. The result is an electronic enrichment of the *d* element present in the IC bimetallic oxides (catalysts increased basicity) and a better catalytic performance for the production of methanol. However, further work is needed in order to confirm such hypothesis for copper based catalysts.

4. Conclusions

Copper-IC bimetallic oxides were tested as catalysts for the production of methanol using greenhouse gases (CO_2 , CH_4) and hydrogen as feedstock. For a better analysis and understanding, their results were compared with those obtained with co-precipitation copper-*f* block element oxide catalysts supported on alumina and with a methanol commercial catalyst. All copper-*f* block element oxides proved to be more active in terms of catalyst intrinsic activity for the production of methanol using CO_2 and H_2 as reagents than the commercial Cu catalyst. The selectivity is also very high (>90%), but the incorporation of CH_4 to the feedstock has a negative effect on the catalyst behavior. The best result was obtained with copper-cerium IC bimetallic oxide; its intrinsic activity ($\approx 900 \text{ mL}_{\text{CH}_3\text{OH}}/\text{m}^2_{\text{Cu}}\cdot\text{h}$) is 2–9 times higher in comparison with the numbers reported in the literature. A possible explanation for such behavior lies in the possibility of a synergetic interaction between CuO and the *f* block element oxide phases that would be responsible for an electronic enrichment of the *d* element and consequent increase in catalytic activity. To our knowledge, copper-*f* block element bimetallic oxides were never tested for the synthesis of methanol. The results herein reported are quite promising, but more studies have to be done aiming, for example, the increase in CO_2 conversion through the preparation of IC bimetallic oxides with higher specific areas.

Acknowledgments

This work was supported by FCT – Portugal under contract number PTDC/AAG-TEC/3324/2012. C2TN/IST authors gratefully acknowledge the FCT – Portugal support through the UID/Multi/04349/2013 project.

Appendix A. Supplementary material

Supplementary data associated with this article can be found, in the online version, at <http://dx.doi.org/10.1016/j.jcat.2016.06.007>.

References

- [1] L. Shi, G. Yang, K. Tao, Y. Yoshiharu, Y. Tan, N. Tsybaki, *Acc. Chem. Res.* 46 (2013) 1838.
- [2] A. Bansode, A. Urakawa, *J. Catal.* 309 (2014) 66.
- [3] J. Graciani, K. Mudiyansele, F. Xu, A.E. Baber, J. Evans, S.D. Senanayake, D.J. Stacchiola, P. Liu, J. Hrbek, J.F. Sanz, J.A. Rodriguez, *Science* 345 (2014) 546.
- [4] E. Pongácz, E. Turpeinen, R. Raudaskoshi, D. Ballivet-Tkatchenko, R.L. Keiski, *Waste Resour. Manage.* 162 (2009) 215.
- [5] G.A. Olah, A. Goepfert, G.K. Surya Prakash, *Beyond Oil and Gas: The Methanol Economy*, Wiley-VCH, Weinheim, Germany, 2006.
- [6] P. Khirsariya, R.K. Mewada, *Procedia Eng.* 51 (2013) 409.
- [7] X.L. Liang, J.R. Xie, Z.M. Liu, *Catal. Lett.* 145 (2015) 1138.
- [8] M. Madej-Lachowska, A. Kasprzyk-Mrzyk, A.I. Lachowski, H. Wyzgol, *CHEMİK* 68 (2014) 61–68.
- [9] Y. Wang, Y. Takahashi, Y. Ohtsuka, *J. Catal.* 186 (1999) 160.
- [10] X.M. Liu, G.Q. Lu, Z.F. Yan, J. Beltramini, *Ind. Eng. Chem. Res.* 42 (2003) 6518.
- [11] W. Wang, S. Wang, X. Ma, J. Gong, *Chem. Soc. Rev.* 40 (2011) 3703.
- [12] K.C. Waugh, *Catal. Lett.* 142 (2012) 1153.
- [13] I. Ganesh, *Renew. Sustain. Energy Rev.* 31 (2014) 221.
- [14] S.G. Jadhav, P.D. Vaidya, B.M. Bhanage, J.B. Joshi, *Chem. Eng. Res. Des.* 92 (2014) 2557.
- [15] M. Behrens, F. Studt, I. Kasatkin, S. Kühn, M. Hävecker, F. Abild-Pedersen, S. Zander, F. Girgsdies, P. Kurr, B.L. Knief, M. Tovar, R.W. Fischer, J.K. Nørskov, R. Schlögl, *Science* 336 (2012) 893.
- [16] M.S. Spencer, *Top. Catal.* 8 (1999) 259.
- [17] (a) I. Kasatkin, P. Kurr, B. Knief, A. Trunschke, R. Schlögl, *Angew. Chem.* 119 (2007) 7465;
(b) M. Behrens, *J. Catal.* 267 (2009) (2009) 24.
- [18] M. Behrens, *J. Catal.* 267 (2009) 24.
- [19] M. Kurtz, H. Wilmer, T. Genger, O. Hinrichsen, M. Muhler, *Catal. Lett.* 86 (2003) 77.
- [20] M. Kurtz, N. Bauer, C. Büscher, H. Wilmer, O. Hinrichsen, R. Becker, S. Rabe, K. Merz, M. Driess, R.A. Fischer, M. Muhler, *Catal. Lett.* 92 (2004) 49.
- [21] J. Yoshihara, C.T. Campbell, *J. Catal.* 161 (1996) 776.
- [22] P.B. Rasmussen, P.M. Holmblad, T. Askgaard, C.V. Ovesen, P. Stoltze, J.K. Nørskov, I. Chorkendorff, *Catal. Lett.* 26 (1994) 373.
- [23] J. Szanyi, D.W. Goodman, *Catal. Lett.* 10 (1991) 383.
- [24] M. Aresta, A. Dibenedetto, *Dalton Trans.* (2007) 2975.
- [25] K. Klier, V. Chatikavanij, R.G. Herman, G.W. Simmons, *J. Catal.* 74 (1982) 343.
- [26] G.C. Chinchin, P.J. Denny, D.G. Parker, M.S. Spencer, D.A. Whan, *Appl. Catal.* 30 (1987) 333.
- [27] M. Sahibzada, *Trans. IChemE* 78A (2000) 943.
- [28] M. Saito, K. Murata, *Catal. Surv. Asia* 8 (2004) 285.
- [29] F. Studt, I. Sharafutdinov, F. Abild-Pedersen, C.F. Elkjær, J.S. Hummelshøj, S. Dahl, I. Chorkendorff, J.K. Nørskov, *Nat. Chem.* 6 (2014) 320.
- [30] C. Liu, B. Yang, E. Tyo, S. Seifert, J. DeBartolo, B. von Issendor, P. Zapol, S. Vajda, L.A. Curtiss, *J. Am. Chem. Soc.* 137 (2015) 8676.
- [31] J. Liu, J. Shi, D. He, Q. Zhang, X. Wu, Y. Liang, Q. Zhu, *Appl. Catal. A: Gen.* 218 (2001) 113.
- [32] J.B. Wang, H.K. Lee, T.J. Huang, *Catal. Lett.* 83 (2002) 79.
- [33] X. Guo, D. Mao, G. Lu, S. Wang, G. Wu, *J. Mol. Catal. A: Chem.* 345 (2011) 60.
- [34] H. Zhan, F. Li, P. Gao, N. Zhao, F. Xiao, W. Wei, L. Zhong, Y. Sun, *J. Power Sources* 251 (2014) 113.
- [35] R. Burch, S.E. Golunski, M.S. Spencer, *J. Chem. Soc., Faraday Trans.* 86 (1990) 2683.
- [36] Y. Kanai, T. Watanabe, T. Fujitani, T. Uchijima, J. Nakamura, *Catal. Today* 28 (1996) 223.
- [37] A.C. Ferreira, A.P. Gonçalves, T.A. Gasche, A.M. Ferraria, A.M. Botelho do Rego, M.R. Correia, A. Margarida Bola, J.B. Branco, *J. Alloys Compd.* 497 (2010) 249.
- [38] J.B. Branco, D. Ballivet-Tkatchenko, A.C. Matos, *J. Mol. Catal. A – Chem.* 307 (2009) 37.
- [39] A.C. Ferreira, A.M. Ferraria, A.M. Botelho do Rego, A.P. Gonçalves, A. Violeta Girão, R. Correia, T. Almeida Gasche, J.B. Branco, *J. Mol. Catal. A – Chem.* 320 (2010) 47.
- [40] Z.R. Ismagilov, S.V. Kuntsevich, N.V. Shikina, V.V. Kuznetsov, M.A. Kerzhentsev, V.A. Ushakov, V.A. Rogov, A.I. Boronin, V.I. Zaikovskiy, *Catal. Today* 157 (2010) 217.
- [41] E.G. Baglin, G.B. Atkinson, L.J. Nicks, *Ind. Eng. Chem. Prod. Res. Dev.* 1 (1981) 87.
- [42] J.B. Branco, T. Almeida Gasche, A.P. Gonçalves, A. Pires de Matos, *J. Alloys Compd.* 323–324 (2001) 610.
- [43] V.R. Choudhary, B.S. Uphade, A.A. Belhekar, *J. Catal.* 163 (1996) 312.
- [44] D. Ballivet-Tkatchenko, J. Branco, A.P. Dematos, *J. Phys. Chem.* 99 (1995) 5481.
- [45] J.B. Branco, T.A. Gasche, A.P. Gonçalves, A.P. de Matos, *J. Alloys Compd.* 323 (2001) 610.
- [46] J. Branco, C. de Jesus Dias, A.P. Gonçalves, T.A. Gasche, A.P. de Matos, *Thermochim. Acta* 420 (2004) 169.
- [47] A.C. Ferreira, A.M. Ferraria, A.M.B. do Rego, A.P. Gonçalves, M.R. Correia, T.A. Gasche, J.B. Branco, *J. Alloys Compd.* 489 (2010) 316.
- [48] A.C. Ferreira, A.P. Gonçalves, T.A. Gasche, A.M. Ferraria, A.M.B. do Rego, M.R. Correia, A.M. Bola, J.B. Branco, *J. Alloys Compd.* 497 (2010) 249.
- [49] J.B. Branco, A.C. Ferreira, A.M. Botelho do Rego, A.M. Ferraria, G. Lopes, T. Almeida Gasche, *ACS Catal.* 2 (2012) 2482.
- [50] J.B. Branco, A.C. Ferreira, Joao.P. Leal, *J. Mol. Catal. A – Chem.* 390 (2014) 45.
- [51] J.B. Branco, A.C. Ferreira, A.M. Botelho do Rego, A.M. Ferraria, G. Lopes, T. Almeida Gasche, *J. Mol. Liq.* 191 (2014) 100.
- [52] J.W. Evans, M.S. Wainwright, A.J. Bridgewater, D.J. Young, *Appl. Catal.* 7 (1983) 75.
- [53] A. Gervasini, S. Bennici, *Appl. Catal. A – Gen.* 281 (2005) 199.
- [54] JCPDS, The Powder Diffraction File, JCPDS, 1601 Park Avenue, Swarthmore, PA, 1981.
- [55] V. Uvarov, I. Popov, *Mater. Charact.* 58 (2007) 883.
- [56] J.P.S. Badyal, R.M. Nix, T. Rayment, R.M. Lambert, *Faraday Discuss. Chem. Soc.* 87 (1989) 121.
- [57] M.F. Luo, Y.J. Zhong, X.X. Yuan, X.M. Zheng, *Appl. Catal. A – Gen.* 162 (1997) 121.
- [58] J.B. Branco, C.J. Dias, A.P. Gonçalves, *J. Alloys Compd.* 478 (2009) 687.
- [59] S. Natesakhawat, J.W. Lekse, J.P. Baltrus, P.R. Ohodnicki Jr., B.H. Howard, X. Deng, C. Matranga, *ACS Catal.* 2 (2012) 1667.
- [60] O. Deutschmann, H. Knozinger, K. Kochloefl, T. Turek, in: *Heterogeneous Catalysis and Solid Catalysts*, Ullmann's Encyclopedia of Industrial Chemistry (2009), http://dx.doi.org/10.1002/14356007.a05_313.pub2, <http://www.itcp.kit.edu/deutschmann/download/III_12_2009_UllmannEncycl_HetCatal_Turek_Deutschmann.pdf>.
- [61] J. Goldstein, D.E. Newbury, D.C. Joy, C. E Lyman, P. Echlin, E. Lifshin, L. Sawyer, J. R. Michael, *Scanning Electron Microscopy and X-ray Microanalysis*, third ed., Springer, 2003. ISBN: 978-0-306-47292-3.
- [62] J.S. Lee, K.I. Moon, S.H. Lee, S.Y. Lee, Y.G. Kim, *Catal. Lett.* 34 (1995) 93.
- [63] D. Jingfa, S. Qi, Z. Yulong, C. Songying, W. Dong, *Appl. Catal. A – Gen.* 139 (1996) 75.
- [64] I.M. Cabrera, M.L. Granados, J.L.G. Fierro, *J. Catal.* 210 (2002) 285.
- [65] J. Toyir, P.R. de la Piscina, J.L.G. Fierro, N. Homs, *Appl. Catal. B – Environ.* 29 (2001) 207.
- [66] J. Toyir, P.R. de la Piscina, J.L.G. Fierro, N. Homs, *Appl. Catal. B – Environ.* 34 (2001) 255.
- [67] J. Liu, J. Shi, D. He, Q. Zhang, X. Wu, Y. Liang, Q. Zhu, *Appl. Catal. A – Gen.* 218 (2001) 113.
- [68] X.M. Liu, G.Q. Lu, Z.F. Yan, *Appl. Catal. A – Gen.* 279 (2005) 241.
- [69] J. Stoczyński, R. Grabowski, A. Kozłowska, P. Olszewski, J. Stoch, J. Skrzypek, M. Lachowska, *Appl. Catal. A – Gen.* 278 (2004) 11.
- [70] X.L. Liang, X. Dong, G.D. Lin, H.B. Zhang, *Appl. Catal. B – Environ.* 88 (2009) 315.